



Contents lists available at ScienceDirect

# Spectrochimica Acta Part A: Molecular and Biomolecular Spectroscopy

journal homepage: [www.journals.elsevier.com/spectrochimica-acta-part-a-molecular-and-biomolecular-spectroscopy](http://www.journals.elsevier.com/spectrochimica-acta-part-a-molecular-and-biomolecular-spectroscopy)



## Chirality transfer observed in Raman optical activity spectra

Ewa Machalska<sup>a,b</sup>, Grzegorz Zajac<sup>b</sup>, Joanna E. Rode<sup>c,1,\*</sup>

<sup>a</sup> Faculty of Chemistry, Jagiellonian University, Gronostajowa 2, 30-38 Krakow, Poland

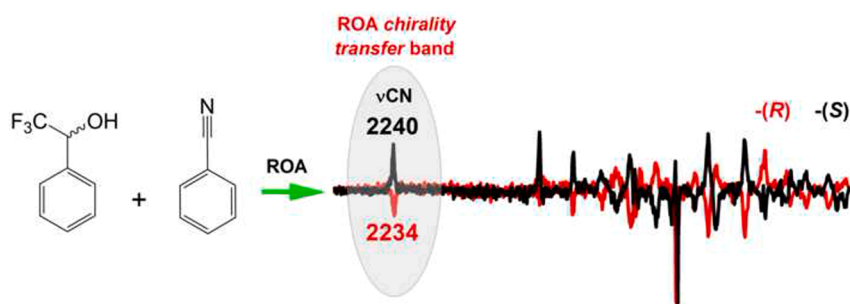
<sup>b</sup> Jagiellonian Centre for Experimental Therapeutics (JCET), Jagiellonian University, Bobrzynskiego 14, 30-348 Krakow, Poland

<sup>c</sup> Institute of Organic Chemistry, Polish Academy of Sciences, Kasprzaka 44/52, 01-224 Warsaw, Poland

### HIGHLIGHTS

- The chirality transfer phenomenon was observed in experimental ROA.
- ROA spectra exhibited  $\nu(\text{CN})$  band of achiral benzonitrile.
- Complexes of chiral solvents with benzonitrile were also studied computationally.

### GRAPHICAL ABSTRACT



### ARTICLE INFO

#### Keywords:

ROA chirality transfer  
Induced chirality  
Chiral solvents  
Calculations

### ABSTRACT

*Chirality transfer* (also called *induced chirality*) is a phenomenon present in chiroptical spectra that manifests itself as a new band or bands of an achiral molecule interacting with a chiral one. In the Raman optical activity (ROA) spectroscopy, the bands of achiral solvents have been recently observed, but the latest papers have shown that they corresponded to the new ECD-Raman (eCP-Raman) effect. Here, we show an unambiguous example of chirality transfer observed in the ROA spectra. The spectra registered for the (1:1) mixtures of achiral benzonitrile with the enantiomers of 2,2,2-trifluoro-1-phenylethanol, 1-phenylethanol, and 1-phenylethylamine exhibited the  $\nu(\text{CN})$  vibration band at about  $2230\text{ cm}^{-1}$ . The ROA measurements were repeated several times to ensure the reliability of the phenomenon. Calculations revealed the  $\text{CN}\cdots\text{HO}$  or  $\text{CN}\cdots\text{HNH}$  hydrogen bond formation accompanied by the  $\pi\cdots\pi$  or  $\text{CH}\cdots\pi$  interactions. The interaction strength was shown to be an important factor for the pronouncement of the ROA chirality transfer effect.

### 1. Introduction

In chiroptical methods such as electronic circular dichroism (ECD), vibrational circular dichroism (VCD), or Raman optical activity (ROA), the absorption/scattering coefficients of the left- and right- circularly

polarized light are different, and as a result, the spectra of the enantiomers are mutual mirror images [1-5]. The methods are especially useful for the unambiguous determination of the absolute configuration of chiral molecules. However, they are also sensitive to the molecular surrounding that influences the band position, its intensity, and even

\* Corresponding author.

E-mail addresses: [ewa.machalska@uj.edu.pl](mailto:ewa.machalska@uj.edu.pl) (E. Machalska), [grzesiek.zajac@uj.edu.pl](mailto:grzesiek.zajac@uj.edu.pl) (G. Zajac), [jrode@icho.edu.pl](mailto:jrode@icho.edu.pl) (J.E. Rode).

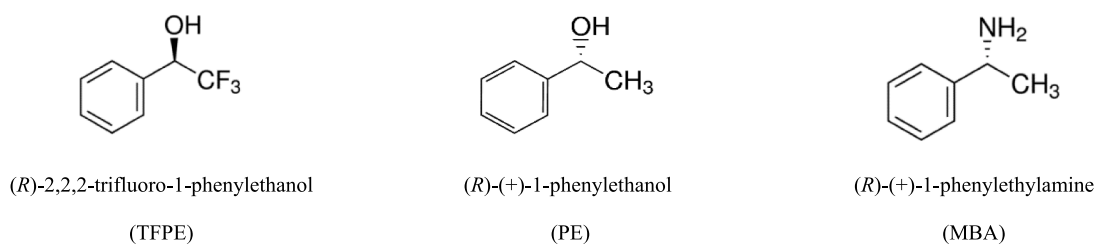
<sup>1</sup> Current address: Institute of Nuclear Chemistry and Technology, 16 Dorodna Street, 03-195 Warsaw, Poland, [j.rode@ichtj.waw.pl](mailto:j.rode@ichtj.waw.pl)

<https://doi.org/10.1016/j.saa.2022.121604>

Received 21 February 2022; Received in revised form 28 June 2022; Accepted 4 July 2022

Available online 8 July 2022

1386-1425/© 2022 The Authors. Published by Elsevier B.V. This is an open access article under the CC BY-NC-ND license (<http://creativecommons.org/licenses/by-nc-nd/4.0/>).



**Scheme 1.** (*R*)-enantiomers of model chiral solutes (different spatial arrangement of the OH group in TFPE and PE is not an error).

sign [6-22]. Therefore, these methods are used in physico-chemical studies. *Chirality transfer* (ChT, or *induced chirality*) is a specific phenomenon present in chiroptical spectra which provides unique information about intermolecular interactions. ChT is manifested as a new band of an achiral molecule that interacts with a chiral one. The phenomenon was first described in the 1970 s for ECD spectra [23,24] and in 2002 for VCD spectroscopy [25,26]. Based on the comparison between the experimental and calculated VCD data, it was possible to gain insight into the hydrogen bonding network surrounding the chiral solute [14,27-33], to distinguish the geometry of the intermolecular complex [26,34] and to indicate the interaction sites [35,36].

In 2012 Dzwolak et al. [37] suggested the transfer of chirality from the protein to ROA-silent solvent due to the strong binding of solvent molecules to the main chain N-H groups with the simultaneous release of the peptide's carbonyl groups. However, as only one enantiomer of the protein could be measured, the mirror image bands were not registered, and thus this is difficult to state if the observed new band was actually the chirality transfer phenomenon, protein conformational change, or other effect. Another reports on the ChT phenomenon in the ROA spectra were initiated by Šebestík *et al.* [38] which probably incorrectly assigned chirality transfer to the ECD-Raman (eCP-Raman) effect [39-43]. Strong ROA bands of achiral nitrile solvent molecules (acetonitrile, acetonitrile-*d*<sub>3</sub>, and liquid HCN) were observed in chiral helquat (HQ) dye [38]. The solvent bands were interpreted as chirality-induced bands resulting from energy transfer from HQ to proximate solvent molecules sharing the HQ electronic space [38]. In 2019, Li et al. also registered ROA bands of different achiral solvents in the presence of the (*R,R*)-bis(pyrrol-2-ylmethyleneamine) cyclohexane nickel(II) complex [44]. The results were interpreted as the chirality transfer phenomenon being a consequence of SERS-like resonance energy transfer processes from a molecular plasmon. In 2021, Machalska et al. registered strong ROA bands of different solvents (both monosigned and bisigned) when characterizing the atropisomeric binaphthalenylamine of *N*-butyl naphthalenediimide (NDI-NH<sub>2</sub>) derivative [45]. The solvent bands dominated the entire ROA spectrum while the chiral NDI-NH<sub>2</sub> bands were barely visible. The unusual ROA enhancement of achiral solvent bands was explained in terms of resonance energy transfer with resonant Raman emission. Moreover, the surprising bisignate RROA sign was interpreted as the result of specific conformational equilibria of the solute in the ground and excited states [45]. However, the last papers of Bouř and co-workers showed that actually the observed phenomenon was a new effect, called ECD-Raman, which was caused by the ECD of colour samples combined with circularly polarized Raman scattering [39-41]. Moreover, in some cases, the ECD-Raman spectra of the solvent could often be stronger than the true RROA spectra of a solute [40]. Notice that the ECD-Raman bands of achiral solvents were often observed in the pre- or resonance conditions.

Here, we showed an unambiguous example of chirality transfer in the ROA spectra. We dissolved achiral benzonitrile (BN) in both forms of three chiral solvents: 2,2,2-trifluoro-1-phenylethanol (TFPE), 1-phenylethanol (PE), and 1-phenylethylamine ( $\alpha$ -methylbenzyl amine, MBA) (Scheme 1). The three solvents are structurally similar but have different abilities for hydrogen bonding with BN. Moreover, they absorb far from the incident beam wavelength (532 nm, Figure S1), making excitation

of the resonance ROA effect hardly possible. Therefore, in such systems, the ECD-Raman effect was also very unlikely [39-43]. The probe benzonitrile molecule exhibited the  $\nu(\text{CN})$  vibration band at 2232 cm<sup>-1</sup>, in the spectral range free from most other vibrational bands. We demonstrated that the ROA ChT phenomenon was strongly dependent on the strength of the interaction between the chiral and achiral molecules.

## 2. Materials and methods

### 2.1. Materials

The highest available quality samples of chiral (*R*)- and (*S*)-2,2,2-trifluoro-1-phenylethanol (also known as  $\alpha$ -(trifluoromethyl)benzyl alcohol or 1-phenyl-2,2,2-trifluoroethanol) were purchased from Apollo Scientific. Both enantiomers of 1-phenylethanol (also known as  $\alpha$ -methylbenzyl alcohol or styrallyl alcohol) and 1-phenylethylamine (also known as  $\alpha$ -methylbenzyl amine), as well as benzonitrile, were bought from Sigma-Aldrich. All compounds were used without further purification.

### 2.2. Raman and ROA measurements

Raman and ROA spectra of both enantiomers of 2,2,2-trifluoro-1-phenylethanol, 1-phenylethanol, and 1-phenylethylamine as well as their (1:1) molar ratio mixtures with achiral benzonitrile were measured using ChiralRAMAN-2X<sup>TM</sup> spectrometer from BioTools Inc. equipped with the 532 nm excitation wavelength laser and the CCD camera. The spectra were accumulated in the 2500–250 cm<sup>-1</sup> spectral range with a resolution of 7 cm<sup>-1</sup>. An integration time of 1 s was used for all samples, except PE-BN system for which it was 3 s. Other specific experimental conditions such as laser power and data collection time were listed in Table S1. Minor baseline corrections of both Raman and ROA spectra were applied. Raw Raman/ROA spectra of the (1:1) systems of benzonitrile with both enantiomers are also provided (Figure S3). To ensure that the ROA chirality transfer was a reliable effect rather than a measurement artifact the experiments were repeated at least two times (Figure S4) for the established conditions (laser power and mixture stoichiometry, see Table S1).

### 2.3. Calculations

Conformational analysis of the studied chiral solvents and their (1:1) and (3:3) molar ratio complexes with benzonitrile was performed applying the Conflex [46] program in which the MMFF94s force field was implemented. Geometry optimizations, Raman, and ROA spectra calculations were performed by using the B3LYP DFT functional [47,48] accounted for the Grimme's DG3 dispersion correction [49], the def2TZVP [50,51] or 6-31G\*\* [52] basis sets applied for (1:1) or (3:3) clusters, and the implicit PCM(benzonitrile) solvent model [53,54]. The stationary structures were found by ascertaining that all of the harmonic frequencies were real. The relative abundances calculated on the SCF or Gibbs free energies (at room temperature) were referred to the value of the most stable system. The spectra were assumed to have Lorentzian shapes with 7 cm<sup>-1</sup> half-width at half-peak height. The intermolecular

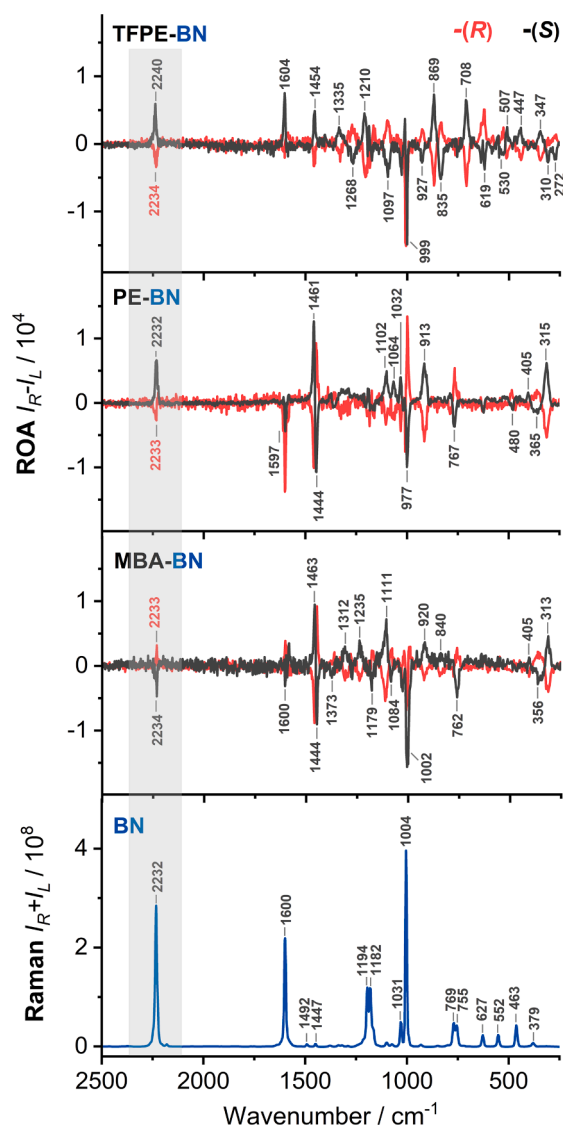


Fig. 1. ROA spectra of both 2,2,2-trifluoro-1-phenylethanol (TFPE), 1-phenylethanol (PE), and 1-phenylethylamine (MBA) dissolved in benzonitrile (BN) in (1:1) molar ratio, as well as the Raman spectrum of pure BN.

interaction energies ( $\Delta E_{\text{int}}$ ) were calculated using the counterpoise method [55] and corrected for the basis set superposition error at the B3LYP-D3/def2TZVP level based on the B3LYP-D3/def2TZVP/PCM geometries. All calculations were performed using the *Gaussian 09* package of programs [56] and the structures were visualized using *GaussView* [57]. The computational data were processed with the help of the *Tesliper* software [58].

### 3. Results and discussion

The aim of this study was to observe the chirality transfer phenomenon by ROA spectroscopy. To this purpose, we registered the ROA spectra of the (1:1) systems of benzonitrile with both enantiomers of 2,2,2-trifluoro-1-phenylethanol (TFPE), 1-phenylethanol (PE), and 1-phenylethylamine (MBA) (Fig. 1). The chiral TFPE, PE, and MBA solvents exhibited distinct abilities for intermolecular interactions and especially the formation of hydrogen bond networks. The sole chiral solvents were the molecules for which the first genuine ROA spectra were measured in the early 1970 s [59–61]. Then, high-quality ROA spectra of MBA and PE were also reported [62,63], and they agreed well with the spectra obtained in this study. However, a good ROA spectrum

of TFPE has not been published until now (Figure S5). The chiral model molecules are structurally similar: PE and MBA differ in the functional groups in the ringside chain: OH vs.  $\text{NH}_2$ , while TFPE and PE have the same OH group but the methyl group in PE is replaced by the trifluoromethyl one in TFPE (Scheme 1).

The Raman spectra of PE and MBA in the 2500–250  $\text{cm}^{-1}$  range are not very influenced by the exchange of the OH and  $\text{NH}_2$  groups (Figure S5). The 1650–1540  $\text{cm}^{-1}$  and 1050–980  $\text{cm}^{-1}$  ranges are almost the same, while minor changes can be detected only between 1400 and 1150  $\text{cm}^{-1}$  (Figure S5). However, altering the  $\text{CH}_3$  with the  $\text{CF}_3$  group significantly modifies the Raman spectra of PE and TFPE particularly below 900  $\text{cm}^{-1}$  (Figure S5). The ROA spectra of chiral MBA and PE solvents also exhibit several similarities, while the spectra of TFPE are noticeably different in the entire spectral range.

The Raman  $\nu(\text{CN})$  band of BN dissolved in PE and MBA is positioned at 2232  $\text{cm}^{-1}$  - the same position as in pure BN (Fig. 1 and S6). A slight blue-shift of  $\nu(\text{CN})$  from 2232 to 2234  $\text{cm}^{-1}$  is observed in the Raman spectrum of BN dissolved in TFPE (Figure S6). The  $\nu(\text{CN})$  band in ROA spectra registered for BN solutions in (R)-TFPE and (R)-PE is positioned at 2234 and 2233  $\text{cm}^{-1}$  respectively (Fig. 1). The  $\nu(\text{CN})$  band is negative for both (R)-TFPE and (R)-PE while positive for (R)-MBA. This peculiar difference in signs was confirmed in several repeated ROA measurements to ensure the reliability of the observed chirality transfer effect (Figure S4). A slight imbalance between the mirror image of ROA  $\nu(\text{CN})$  bands was observed for TFPE–BN and PE–BN mixtures: the positive bands were higher in intensity than their negative counterparts (Fig. 1). We have measured the ROA spectra of achiral benzonitrile several times to ensure the  $\nu(\text{CN})$  band artifact was not accidentally positive (Figure S6). The positive ChT ROA  $\nu(\text{CN})$  bands of higher intensity registered for mixtures resulted from benzonitrile artifact and chirality induced signals overlapping. It could happen that, using for example a different setup of the spectrometer, a real ChT band would be dominated by the oppositely directed solvent artifact, and finally, the ChT band sign would be inverted to a wrong value. However, no mirror image ChT pattern would be obtained for enantiomers in such a case. The fact that  $\nu(\text{CN})$  band of BN is observed and that it is reflected as a mirror image when the enantiomeric form of the solvent is changed, definitely confirms the presence of the chirality transfer effect in the ROA spectra.

Presence of BN in the chiral TFPE, PE, and MBA solvents modify the Raman spectral pattern at ca. 1600  $\text{cm}^{-1}$ , as well as in the ranges between 1250 and 1140  $\text{cm}^{-1}$  and below 900  $\text{cm}^{-1}$ . On the other hand, the ROA signals at ca. 1600  $\text{cm}^{-1}$  and 1000  $\text{cm}^{-1}$  seem to be mostly artifacts originating from the strong polarized Raman bands of both achiral benzonitrile and chiral compounds, which probably dominate over the intensity of the possible signals due to the chirality induction.

Now, consider the BN-chiral solvent systems from computational point of view. The addition of benzonitrile to 2,2,2-trifluoro-1-phenylethanol, 1-phenylethanol, and 1-phenylethylamine solvents perturbs their hydrogen bond networks, first of all by competing in the hydrogen bonds in the role of hydrogen bond acceptor. Therefore, the energy of the binary solvent–solvent interactions compared to the binary solute–solvent interactions is crucial. The higher the binary solute–solvent interactions, the more pronounced effect on the ROA spectra is expected. However, binary interactions yield only the first approximation of the real systems and cannot explain all the details that may happen in the systems. First, consider the stabilization energy of the binary BN-chiral solvent systems. Estimating the stabilization energy for the BN (1:1) complexes with flexible TFPE, PE, and MBA molecules requires calculations of all conformations of the (1:1) complexes. MBA, PE, and TFPE molecules have different abilities for hydrogen bonding and accompanying interactions: the  $\text{NH}_2$  group is an electron donor group, the OH group is mostly a proton donor group, while the  $\text{CF}_3$  one (an efficient electron-withdrawing group [64]) makes the OH group in TFPE more acidic than in PE. As a result, the strongest interactions with the proton-accepting CN group were expected to occur in TFPE, while the weakest - in MBA. Potentially, benzonitrile has three proton accepting sites: first of

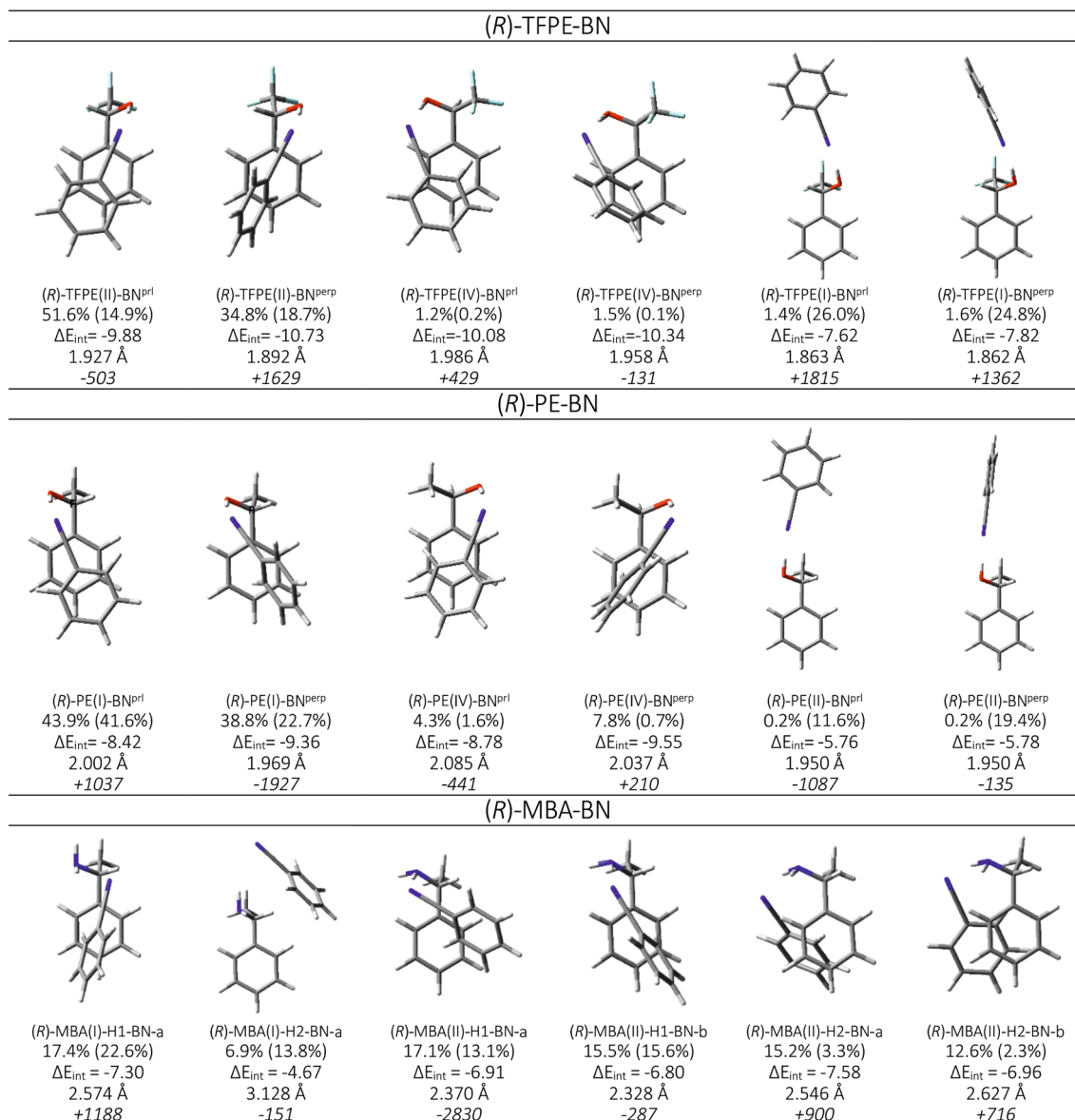


**Fig. 2.** The selected (1:1) (R)-TFPE-BN (top), (R)-PE-BN (middle), and (R)-MBA-BN (bottom) complexes followed by the SCF populations (Gibbs values in parentheses), interaction energies ( $\Delta E_{int}$ , kcal/mol) and the intermolecular CN...OH or CN...NH<sub>2</sub> bond lengths. The relationship of the complex structures with the intensities of the ROA chirality transfer  $\nu(\text{CN})$  band ( $10^4$  K) is indicated in the last line. Calculations were performed at the B3LYP-D3/def2TZVP/PCM level.

all the lone electron pair at the CN nitrogen atom, but also the triple bond of the CN group, and the  $\pi$  electrons of the phenyl ring. Furthermore, hydrogen atoms in the BN ring may interact forming weak C-H... $\pi$  hydrogen bonds [65]. However, in all calculated (1:1) complexes, hydrogen bonds were formed between the CN group and the OH or NH<sub>2</sub> groups (Fig. 2 and S7-S9). Nevertheless, most structures were additionally stabilized by the  $\pi$ ... $\pi$  or CH... $\pi$  interactions. Notice that BN adopted two geometries, parallel (*prl*) or perpendicular (*perp*), with respect to the ring of the chiral molecule. Stabilization energies of the TFPE-BN and PE-BN complexes strongly depended on whether the SCF or Gibbs free energies were considered (Tables S2 and S3). The SCF level, at which the systems are minimized, favoured structures with the CN...HO hydrogen bonds accompanied by the  $\pi$ ... $\pi$  or CH... $\pi$  interactions. Such structures accounted for ca. 90% of both TFPE-BN and PE-BN systems (Tables S2 and S3). On the other hand, the Gibbs energies indicated the high percentage of structures with solely linear HB-bonds accounted for ca. 50% and 30% in the TFPE-BN and PE-BN complexes, respectively (Tables S2 and S3).

The interaction energy averaged over the population unequivocally

**Table 1**

Position of the ROA chirality transfer  $\nu(\text{CN})$  band (freq, cm<sup>-1</sup>), its intensities (ROA, 10<sup>4</sup> K), and interaction strength ( $\Delta E_{int}$ , kcal/mol) calculated for the (1:1) intermolecular complexes studied as average over the SCF or Gibbs free energy population factors at the B3LYP-D3/def2TZVP/PCM level.

	SCF			Gibbs		
	freq*	ROA	$\Delta E_{int}$	freq*	ROA	$\Delta E_{int}$
(R)-TFPE-BN	2324.2	391.7	-10.03	2333.3	951.3	-8.73
(R)-PE-BN	2323.0	-309.8	-8.90	2324.5	-255.7	-7.81
(R)-MBA-BN	2322.8	-41.8	-6.94	2322.5	-138.5	-6.34

\* the calculated sole benzonitrile  $\nu(\text{CN})$  band position is 2322.9 cm<sup>-1</sup>.

indicated that the interactions were the strongest for TFPE, medium for PE, and the weakest for MBA (Tables 1 and S2-S4). Noticeably, the position of the population-averaged chirality transfer  $\nu(\text{CN})$  band behaved similarly as observed in the experimental spectra. It was quite the same for MBA and PE, while slightly blue-shifted for TFPE. However, the SCF

energy averaging suggested a blue-shift of *ca.* 1 cm<sup>-1</sup> while the Gibbs free energy averaging was *ca.* 10 cm<sup>-1</sup> (Table 1). On the other hand, the position of the  $\nu(\text{CN})$  band remained practically unchanged for MBA and PE (Table 1).

The computational ROA intensities of the chirality transfer  $\nu(\text{CN})$  band of (1:1) complexes, whether SCF or Gibbs free energy averaged, mostly disagree with those found experimentally (Table 1, Figures 1 and S10). The computations suggest that the  $\nu(\text{CN})$  band is positive when BN is dissolved in TFPE, while it is negative for PE and MBA, whereas experimental spectra show the negative band for both TFPE and PE while it is positive for MBA. Notice that the  $\nu(\text{CN})$  band sign strongly depend on the mutual orientation of two aromatic rings (Fig. 2 and Tables S2-S4). We also considered larger (3:3) clusters; however, these calculations did not reproduce the  $\nu(\text{CN})$  band sign of the TFPE-BN system as well (Figures S12-S15, Tables S5-S7). On the other hand, the results shed some light on the probable explanation of unexpected differences in the  $\nu(\text{CN})$  band sign observed for the MBA-BN system. The NH<sub>2</sub> group, an electron and proton donor, can interact simultaneously with one or more benzonitrile molecules, other MBA molecules, or both of them (Figure S15). Thus, the net of intermolecular interactions present in the MBA-BN system is different than for the chiral molecules with the OH group (Figures S13-S15). In fact, in real systems much more complicated clusters of interacting molecules occur. In the future, we plan to perform molecular-dynamic calculations for a better description of the bonding networks in which both the hydrogen bond and  $\pi$  interactions take place. However, such a task was beyond the scope of this study.

#### 4. Conclusions

In this study, we observed the ROA chirality transfer manifested by presence of the  $\nu(\text{CN})$  band of achiral benzonitrile dissolved in both enantiomers of 2,2,2-trifluoro-1-phenylethanol (TFPE), 1-phenylethanol (PE), and 1-phenylethylamine (MBA). Several ROA measurements were performed to ensure the reliability of the observed effect. To our knowledge, this is the first observation of the ROA chirality transfer with the mirror image pattern of the observed ROA ChT band.

The benzonitrile's  $\nu(\text{CN})$  Raman band was placed at *ca.* 2232 cm<sup>-1</sup> in PE and MBA. A slight blue-shift of  $\nu(\text{CN})$  was observed for BN dissolved in TFPE. The (1:1) complexes of BN with TFPE, PE, and MBA calculated at the DFT level revealed the most important role of the hydrogen bonds formed between the CN group and the OH or NH<sub>2</sub> groups. Most structures were also stabilized by the  $\pi\cdots\pi$  or CH $\cdots\pi$  interactions. The interaction strength changed in the TFPE > PE > MBA order. The population-averaged ROA chirality transfer  $\nu(\text{CN})$  band position fairly matched the experimental behaviour. For the PE-BN and MBA-BN systems, the obtained  $\nu(\text{CN})$  ROA band sign matched the measured one when the (3:3) chiral/achiral BN clusters were considered. We showed that the  $\nu(\text{CN})$  band sign strongly depended on the mutual orientation of two aromatic rings, thus, better description of the bonding networks in which both the hydrogen bond and  $\pi$ - $\pi$  interactions take place is required. Such a task was beyond the scope of this study, however, it is believed the ROA chirality transfer will become a recognized method in physicochemical studies of intermolecularly interacting systems.

#### Funding

This work was supported by the Polish National Science Centre Grant No. UMO-2015/19/B/ST4/03759.

#### CRediT authorship contribution statement

**Ewa Machalsk:** Methodology, Software, Investigation, Writing – original draft, Writing – review & editing, Visualization. **Grzegorz Zajac:** Methodology, Writing – review & editing. **Joanna E. Rode:** Methodology, Software, Investigation, Writing – original draft, Writing –

review & editing, Visualization, Project administration, Funding acquisition.

#### Declaration of Competing Interest

The authors declare that they have no known competing financial interests or personal relationships that could have appeared to influence the work reported in this paper.

#### Acknowledgments

This work was supported by the Polish National Science Centre Grant No. UMO-2015/19/B/ST4/03759. The PL-Grid infrastructure is acknowledged for computing time.

#### Appendix A. Supplementary material

Supplementary data to this article can be found online at <https://doi.org/10.1016/j.saa.2022.121604>.

#### References

- [1] P.L. Polavarapu, *Chiroptical spectroscopy: fundamentals and applications*, Taylor & Francis, 2016.
- [2] N. Eds, P.L. Berova, K. Polavarapu, R.W. Nakanishi, *Comprehensive chiroptical spectroscopy*, John Wiley & Sons Inc, Woody, 2012.
- [3] L.A. Nafie, *Vibrational optical activity: principles and applications*, John Wiley & Sons Inc, 2011.
- [4] M. Krupová, J. Kessler, P. Bouř, Recent trends in chiroptical spectroscopy: theory and applications of vibrational circular dichroism and raman optical activity, *ChemPhysChem*. 22 (2021) 83–91, <https://doi.org/10.1002/cplu.202000014>.
- [5] G. Magyarfalvi, G. Tarczay, E. Vass, Vibrational circular dichroism, *WIREs Comput. Mol. Sci.* 1 (2011) 403–425, <https://doi.org/10.1002/wcms.39>.
- [6] E. Debie, P. Bultinck, W. Herrebout, B. Van der Veken, Solvent effects on IR and VCD spectra of natural products: an experimental and theoretical VCD study of pulegone, *Phys. Chem. Chem. Phys.* 10 (2008) 3498–3508, <https://doi.org/10.1039/B801313F>.
- [7] S. Göbi, E. Vass, G. Magyarfalvi, G. Tarczay, Effects of strong and weak hydrogen bond formation on VCD spectra: a case study of 2-chloropropionic acid, *PhysChemChemPhys*. 13 (2011) 13972–13984, <https://doi.org/10.1039/C1CP20797K>.
- [8] V.P. Nicu, E.J. Baerends, P.L. Polavarapu, Understanding solvent effects in vibrational circular dichroism spectra: [1,1'-Binaphthalene]-2,2'-diol in dichloromethane, acetonitrile, and dimethyl sulfoxide solvents, *J. Phys. Chem. A* 116 (2012) 8366–8373, <https://doi.org/10.1021/jp303891x>.
- [9] C. Merten, C.J. Berger, R. McDonald, Y. Xu, Evidence of dihydrogen bonding of a chiral amine-borane complex in solution by VCD spectroscopy, *Angew. Chem. Int. Ed.* 53 (2014) 9940–9943, <https://doi.org/10.1002/anie.201403690>.
- [10] A.S. Perera, J. Thomas, M. Reza Poopari, Y. Xu, The clusters-in-a-liquid approach for solvation: new insights from the conformer specific gas phase spectroscopy and vibrational optical activity spectroscopy, *Front. Chem.* 4 (2016) 1–17, <https://doi.org/10.3389/fchem.2016.00009>.
- [11] D.P. Demarque, C. Merten, Intra- vs. intermolecular hydrogen bonding: Solvent-dependent conformational preferences of a common supramolecular binding motif from <sup>1</sup>H-NMR and VCD spectra, *Chem. Eur. J.* 23 (2017) 17915–17922, <https://doi.org/10.1002/chem.201703643>.
- [12] C. Merten, Vibrational optical activity as probe for intermolecular interactions, *Phys Chem. Chem. Phys.* 19 (2017) 18803–18812, <https://doi.org/10.1039/C7CP02544K>.
- [13] A.S. Perera, J. Cheramy, C. Merten, J. Thomas, Y. Xu, IR, raman and vibrational optical activity spectra of methyl glycidate in chloroform and water: the clusters-in-a-liquid solvation model, *ChemPhysChem*. 19 (2018) 2234–2242, <https://doi.org/10.1002/cphc.201800309>.
- [14] L. Weirich, C. Merten, Solvation and self-aggregation of chiral alcohols: How hydrogen bonding affects their VCD spectral signatures, *Phys. Chem. Chem. Phys.* 21 (2019) 13494–13503, <https://doi.org/10.1039/C9CP01407A>.
- [15] L. Weirich, J. Magalhães de Oliveira, C. Merten, How many solvent molecules are required to solvate chiral 1,2-diols with hydrogen bonding solvents? A VCD spectroscopic study, *Phys. Chem. Chem. Phys.* 22 (2020) 1525–1533, <https://doi.org/10.1039/C9CP06030H>.
- [16] S. Ghidinelli, S. Abbate, J. Koshoubu, Y. Araki, T. Wada, G. Longhi, Solvent Effects and Aggregation Phenomena Studied by Vibrational Optical Activity and Molecular Dynamics: The Case of Pantolactone, *J. Phys. Chem. B* 124 (2020) 4512–4526, <https://doi.org/10.1021/acs.jpcc.0c01483>.
- [17] K.H. Hopmann, K. Ruud, M. Pecul, A. Kudelski, M. Dračinský, P. Bouř, Explicit versus implicit solvent modeling of Raman optical activity spectra, *J. Phys. Chem. B* 115 (2011) 4128–4137, <https://doi.org/10.1021/jp110662w>.

- [18] S. Lubber, Solvent effects in calculated vibrational raman optical activity spectra of  $\alpha$ -helices, *J. Phys. Chem. A* 117 (2013) 2760–2770, <https://doi.org/10.1021/jp400105u>.
- [19] A.N.L. Batista, J.M. Batista Jr, V.S. Bolzani, M. Furlan, E.W. Blanch, Selective DMSO-induced conformational changes in proteins from Raman optical activity, *Phys. Chem. Chem. Phys.* 15 (2013) 20147–20152, <https://doi.org/10.1039/c3cp53525h>.
- [20] J.E. Rode, M. Górecki, S. Witkowski, J. Frelek, Solvation of 2-(hydroxymethyl)-2,5,7,8-tetramethyl-chroman-6-ol revealed by circular dichroism: a case of chromane helicity rule breaking, *PhysChemChemPhys.* 20 (2018) 22525–22536, <https://doi.org/10.1039/C8CP02491J>.
- [21] A. Robinson de Souza, V. Farias Ximenes, N. Henrique Morgon, Solvent Effects on Electronic Circular Dichroism Spectra, in *Stereochemistry and Global Connectivity: The Legacy of Ernest L. Eliel Volume 2* Eds. H. N. Cheng, C. A. Maryanoff, B. D. Miller, D. Grob Schmidt, ACS Symposium Series Vol. 1258, Copyright © 2017, American Chemical Society, DOI: 10.1021/bk-2017-1258.ch007.
- [22] E. Machalska, G. Zając, M. Baranska, P. Bouř, D. Kaczorek, R. Kawęcki, J. E. Rode, K. Lyczko, J. Cz. Dobrowolski, New chiral ECD-Raman spectroscopy of atropisomeric naphthalenediimides, *Chem. Commun.*, under review.
- [23] S. Mason, Induced circular dichroism, *Chem. Phys. Lett.* 32 (1975) 201–203, [https://doi.org/10.1016/0009-2614\(75\)85103-7](https://doi.org/10.1016/0009-2614(75)85103-7).
- [24] S. Allenmark, Induced circular dichroism in chiral molecular interaction, *Chirality* 15 (2003) 409–422, <https://doi.org/10.1002/chir.10220>.
- [25] T. Burgi, A. Vargas, A. Baiker, VCD spectroscopy of chiral cinchona modifiers used in heterogeneous enantioselective hydrogenation: conformation and binding of non-chiral acids, *J. Chem. Soc., Perkin Trans. 2* (2002) 1596–1601, <https://doi.org/10.1039/B203251A>.
- [26] J.E. Rode, J. Cz. Dobrowolski, VCD technique in determining intermolecular H-bond geometry: a DFT study, *J. Mol. Struct. (THEOCHEM)* 637 (2003) 81–89, [https://doi.org/10.1016/S0166-1280\(03\)00366-X](https://doi.org/10.1016/S0166-1280(03)00366-X).
- [27] M. Losada, X.u. Yunjie, Chirality transfer through hydrogen-bonding: experimental and ab initio analyses of vibrational circular dichroism spectra of methyl lactate in water, *Phys. Chem. Chem. Phys.* 9 (2007) 3127–3135, <https://doi.org/10.1039/B703368K>.
- [28] E. Debie, L. Jaspers, P. Bultinck, W. Herrebout, B. van der Veken, Induced solvent chirality: a VCD study of camphor in CDCl<sub>3</sub>, *Chem. Phys. Lett.* 450 (2008) 426–430, <https://doi.org/10.1016/j.cplett.2007.11.064>.
- [29] G. Yang, Y. Xu, Probing chiral solute-water hydrogen bonding networks by chirality transfer effects: a vibrational circular dichroism study of glycidol in water, *J. Chem. Phys.* 130 (2009), <https://doi.org/10.1063/1.3116582>, 164506/1-9.
- [30] J. Sadlej, J. Cz. Dobrowolski, J.E. Rode, VCD spectroscopy as a novel probe for chirality transfer in molecular interactions, *Chem. Soc. Rev.* 39 (2010) 1478–1488, <https://doi.org/10.1039/B915178H>.
- [31] M.R. Poopari, P. Zhu, Z. Dezhahang, Yunjie Xu, Vibrational absorption and vibrational circular dichroism spectra of leucine in water under different pH conditions: hydrogen-bonding interactions with water, *J. Chem. Phys.* 137 (2012) 194308/1-7, <https://doi.org/10.1063/1.4767401>.
- [32] J. Cz. Dobrowolski, J. E. Rode, J. Sadlej, Chapter 15: VCD Chirality Transfer: A New Insight into the Intermolecular Interactions, pp. 451–477 in *Practical Aspects of Computational Chemistry I: An Overview of the Last Two Decades and Current Trends*, J. Leszczynski, M. K. Shukla (eds.) (c) Springer Science+Business Media B. V. 2012.
- [33] P. Daniel, Demarque, Michael Kemper, Christian Merten, VCD spectroscopy reveals that a water molecule determines the conformation of azithromycin in solution, *Chem. Commun.* 57 (2021) 4031–4034, <https://doi.org/10.1039/D1CC00932J>.
- [34] C. Merten, Y. Xu, Chirality transfer in the methyl lactate-ammonia complex observed by matrix-isolation vibrational circular dichroism spectroscopy, *Angew. Chem. Int. Ed.* 52 (2013) 2073–2076, <https://doi.org/10.1002/anie.201208685>.
- [35] J.E. Rode, M.H. Jamróz, J. Sadlej, J. Cz. Dobrowolski, On VCD chirality transfer in EDA complexes. a prediction for the quinine--BF<sub>3</sub> system, *J. Phys. Chem. A* 116 (2012) 7916–7926, <https://doi.org/10.1021/jp304955v>.
- [36] J.E. Rode, J. Cz. Dobrowolski, On chirality transfer in electron-donor-acceptor complexes. a prediction for the sulfonimine--BF<sub>3</sub> system, *Chirality* 24 (2012) 5–16, <https://doi.org/10.1021/jp304955v>.
- [37] W. Dzwolak, J. Kalinowski, C. Johannessen, V. Babenko, G. Zhang, T. Keiderling, On the DMSO-Dissolved State of Insulin: A Vibrational Spectroscopic Study of Structural Disorder, *J. Phys. Chem. B* 116 (2012) 11863, <https://doi.org/10.1021/jp3062674>.
- [38] J. Šebestík, F. Teplý, F.I. Císařová, J. Vávra, D. Koval, P. Bouř, Intense chirality induction in nitrile solvents by a helquat dye monitored by near resonance Raman scattering, *Chem. Commun.* 52 (2016) 6257–6260, <https://doi.org/10.1039/C6CC01606E>.
- [39] T. Wu, G. Li, J. Kapitán, J. Kessler, Y. Xu, P. Bouř, Two spectroscopies in one: interference of circular dichroism and raman optical activity, *Angew. Chem. Int. Ed.* 59 (2020) 21789, <https://doi.org/10.1002/anie.202011146>.
- [40] E. Machalska, G. Zając, A.J. Wierzba, J. Kapitán, T. Andrúniów, M. Spiegel, D. Gryko, P. Bouř, M. Baranska, Recognition of the true and false resonance raman optical activity, *Angew. Chem. Int. Ed.* 60 (2021) 21205–21210, <https://doi.org/10.1002/anie.202107600>.
- [41] G. Li, M. Alshalalfeh, Y. Yang, J.R. Cheeseman, P. Bouř, Y. Xu, Can One Measure Resonance Raman Optical Activity? *Angew. Chem. Int. Ed.* 60 (2021) 22004–22009, <https://doi.org/10.1002/anie.202109345>.
- [42] G. Zając, P. Bouř, Measurement and Theory of Resonance Raman Optical Activity for Gases, Liquids, and Aggregates. What It Tells about Molecules, *J. Phys. Chem. B* 126 (2022) 355–367, <https://doi.org/10.1021/acs.jpcc.1c08370>.
- [43] G. Li, M. Alshalalfeh, J. Kapitán, P. Bouř, Y. Xu, Electronic circular dichroism-circularly polarized Raman (eCP-Raman): a new form of chiral Raman spectroscopy, *Chem. Eur. J.* (2022), e202104302, <https://doi.org/10.1002/chem.202104302>.
- [44] G. Li, J. Kessler, J. Cheramy, T. Wu, M.R. Poopari, P. Bouř, Y. Xu, Transfer and amplification of chirality within the “ring of fire” observed in resonance raman optical activity experiments, *Angew. Chem. Int. Ed.* 58 (2019) 16495–16498, <https://doi.org/10.1002/anie.201909603>.
- [45] E. Machalska, G. Zając, M. Baranska, D. Kaczorek, R. Kawęcki, P.F.J. Lipiński, J. E. Rode, J. Cz. Dobrowolski, On Raman optical activity sign-switching between the ground and excited states leading to an unusual resonance ROA induced chirality, *Chem. Sci.* 12 (2021) 911–916, <https://doi.org/10.1039/D0SC05345G>.
- [46] CONFLX 7, Conflex Corp., Japan, 2012.
- [47] A.D. Becke, Density-functional exchange-energy approximation with correct asymptotic behavior, *Phys. Rev. A* 38 (1988) 3098–3100, <https://doi.org/10.1103/PhysRevA.38.3098>.
- [48] C. Lee, W. Yang, R.G. Parr, Development of the Colle-Salvetti correlation-energy formula into a functional of the electron density, *Phys. Rev. B* 37 (1988) 785–789, <https://doi.org/10.1103/PhysRevB.37.785>.
- [49] S. Grimme, J. Antony, S. Ehrlich, H. Krieg, A consistent and accurate ab initio parametrization of density functional dispersion correction (DFT-D) for the 94 elements H-Pu, *J. Chem. Phys.* 132 (2010), <https://doi.org/10.1063/1.3382344>, 154104/1-15.
- [50] F. Weigend, R. Ahlrichs, R., Balanced basis sets of split valence, triple zeta valence and quadruple zeta valence quality for H to Rn: Design and assessment of accuracy, *Phys. Chem. Chem. Phys.* 7 (2005) 3297–3305, <https://doi.org/10.1039/B508541A>.
- [51] F. Weigend, Accurate coulomb-fitting basis sets for H to Rn, *Phys. Chem. Chem. Phys.* 8 (2006) 1057–1065, <https://doi.org/10.1039/B515623H>.
- [52] V.A. Rassolov, M.A. Ratner, J.A. Pople, P.C. Redfern, L.A. Curtiss, 6–31G\* basis set for third-row atoms, *J. Comp. Chem.* 22 (2001) 976–984, <https://doi.org/10.1002/jcc.1058>.
- [53] B. Mennucci, Polarizable continuum model, *Wiley Interdiscip. Rev.: Comput. Mol. Sci.* 2 (2012) 386–404, <https://doi.org/10.1002/wcms.1086>.
- [54] G. Scalmani, M.J. Frisch, Continuous surface charge polarizable continuum models of solvation. I. General formalism *J. Chem. Phys.* 132 (2010), 114110, <https://doi.org/10.1063/1.3359469>.
- [55] S.F. Boys, F. Bernardi, The calculation of small molecular interactions by the differences of separate total energies. some procedures with reduced errors, *Mol. Phys.* 19 (1970) 553–566, <https://doi.org/10.1080/00268977000101561>.
- [56] M. J. Frisch, G. W. Trucks, H. B. Schlegel, G. E. Scuseria, M. A. Robb, J. R. Cheeseman, G. Scalmani, V. Barone, B. Menucci, G. A. Petersson, H. Nakatsuji, M. Caricato, X. Li, H. P. Hratchian, A. F. Izmaylov, J. Bloino, G. Zheng, J. L. Sonnenberg, M. Hada, M. Ehara, K. Toyota, R. Fukuda, J. Hasegawa, M. Ishida, T. Nakajima, Y. Honda, O. Kitao, H. Nakai, T. Vreven, J. A. Montgomery, Jr, J. E. Peralta, F. Ogliaro, M. Bearpark, J. J. Heyd, E. Brothers, K. N. Kudin, V. N. Staroverov, T. Keith, R. Kobayashi, J. Normand, K. Raghavachari, A. Rendell, J. C. Burant, S. S. Iyengar, J. Tomasi, M. Cossi, N. Rega, J. M. Millam, M. Klene, J. E. Knox, J. B. Cross, V. Bakken, C. Adamo, J. Jaramillo, R. Gomperts, R. E. Stratmann, O. Yazyev, A. J. Austin, R. Cammi, C. Pomelli, J. W. Ochterski, R. L. Martin, K. Morokuma, V. G. Zakrzewski, G. A. Voth, P. Salvador, J. J. Dannenberg, S. Dapprich, A. D. Daniels, O. Farkas, J. B. Foresman, J. V. Ortiz, J. Cioslowski, D. J. Fox, Gaussian 09, Re-vision D.01, Gaussian, Inc., Wallingford CT, US, 2010.
- [57] R. D. Dennington II, T. A. Keith, J. E. Millam, GaussView 6.0.16, Semicem Inc. 2000-2016.
- [58] M. M. Węciław, Tesliper: a theoretical spectroscopist's little helper, *Journal of Open Source Software*, 7 (2022) 4164, [10.21105/joss.04164](https://doi.org/10.21105/joss.04164).
- [59] L.D. Barron, M.P. Bogaard, A.D. Buckingham, Raman scattering of circularly polarized light by optically active molecules, *J. Am. Chem. Soc.* 95 (1973) 603–605, <https://doi.org/10.1021/ja00783a058>.
- [60] W. Hug, S. Kint S, G.F. Bailey, J.R. Scherer, Raman circular intensity differential spectroscopy. the spectra of (2)- $\alpha$ -pinene and (1)- $\alpha$ -phenylethylamine, *J. Am. Chem. Soc.* 97 (1975) 5598–15590, <https://doi.org/10.1021/ja00852a049>.
- [61] L.D. Barron, Raman optical activity of simple chiral molecules; methyl and trifluoromethyl asymmetric deformations, *J. Chem. Soc. Perkin Trans. 2* (1977) 1790–1794, <https://doi.org/10.1039/P29770001790>.
- [62] L.D. Barron, The development of biomolecular Raman optical activity spectroscopy, *Biomed. Spectroscopy and Imaging* 4 (2015) 223–253, <https://doi.org/10.3233/BSI-150113>.
- [63] J. Kapitán, C. Johannessen, P. Bouř, L. Hecht, L.D. Barron, Vibrational raman optical activity of 1-phenylethanol and 1-phenylethylamine: revisiting old friends, *Chirality* 21 (2009) E4–E12, <https://doi.org/10.1002/chir.20747>.
- [64] T. Siodła, W.P. Ozimiński, M. Hoffmann, H. Koroniak, Toward a physical interpretation of substituent effects: the case of fluorine and trifluoromethyl groups, *J. Org. Chem.* 79 (2014) 7321–7331, <https://doi.org/10.1021/jo501013p>.
- [65] D.R. Borst, D.W. Pratt, M. Schaeffer, Molecular recognition in the gas phase. dipole-bound complexes of benzonitrile with water, ammonia, methanol, acetonitrile, and benzonitrile itself, *Phys. Chem. Chem. Phys.* 9 (2007) 4563, <https://doi.org/10.1039/B705679F>.